Itraconazole: A Promising Repurposed Chemotherapeutic Agent for Tongue Carcinoma

Hala A. El-kammar[1], Mohamed M. Ammar[2], Iten M. Fawzy[3], Dina M. Abdelkhalek[4] and Nermeen S. Afifi[4]

Original Article

[1]Department of Oral Pathology, Faculty of Oral and Dental Medicine, Future University in Egypt, Cairo, Egypt

[2]Department of Dental Biomaterials, Faculty of Oral and Dental Medicine, Future University in Egypt, Cairo, Egypt

[3]Department of Pharmaceutical Chemistry, Faculty of Pharmacy, Future University in Egypt, Cairo, Egypt

[4]Department of Oral Biology, Faculty of Dentistry, Ain Shams University, Cairo, Egypt

ABSTRACT

Introduction: Researching novel chemotherapeutic agents is desirable but it is not ideal in terms of cost and time, hence, repurposing current drugs for cancer treatment is becoming more appealing. Itraconazole (ITZ), traditionally an anti-fungal drug has been re-purposed recently as an anticancer agent for many cancer types. There is continuous bidirectional and intricate crosstalk between cancer-associated fibroblasts (CAFs) and cancer cells. Most emerging trends in CAF biology draw attention to CAF-secreted factors as druggable targets. PI3/AKT signaling has been linked to both α-SMA and TGF-β expressions and CAFs differentiation and is a key player in, chemotherapeutic resistance.

Objectives: This study aimed to correlate the immunohistochemical expression of α-SMA as a marker for CAF and TGF-β with tumor grade and lymph node involvement in tongue squamous cell carcinoma (TSCC) specimens and to evaluate the effect of ITZ on invasion and migration of TSCC cell line.

Materials and Methods: Immunohistochemical expression of α-SMA and TGF-β in twenty-four samples of different grades of TSCC and clinical lymph node involvement were evaluated retrospectively. Molecular docking of ITZ with PI3/AKT was performed and its effect on SCC-25 cell line cultured in medium obtained from co-culture of WI-38 (normal fibroblast) and SCC-25 cell lines was assessed. Expression of α-SMA, TGF-β, SNAIL and VEGF genes as well as invasion and migration ability were evaluated.

Results: Immunohistochemical expression of α-SMA and TGF-β was significantly higher in cases exhibiting lymph node involvement. ITZ interacted strongly with PI3/AKT proteins ITZ-treated group showed significantly lower migration and invasion ability as well as α-SMA, TGF-β, SNAIL and VEGF expressions compared to control group.

Conclusion: ITZ was able to inhibit invasion and migration of TSCC cell line in *vitro*.

Received: 31 January 2023, **Accepted:** 14 March 2023

Key Words: α-SMA, cancer associated fibroblasts, PI3/AKT, SNAIL, TGF-β.

Corresponding Author: Nermeen Sami Afifi, PhD, Department of Oral Pathology, Faculty of Dentistry, Ain Shams University, Egypt, **Tel.**: +20 11 4549 3033, **E-mail:** nermasami@dent.asu.edu.eg

ISSN: 1110-0559, Vol. 47, No. 1

INTRODUCTION

The incidence of tongue squamous cell carcinoma (TSCC) is nowadays higher than that of other oral squamous cell carcinoma (OSCC) sites, particularly among people aged 20 to 44. The presence of lymph node (LN) involvement is one of the most important independent prognostic variables in TSCC[1,2].

Metastasis is a multistep process involving epithelial-mesenchymal transition (EMT) and tumor neo-angiogenesis[3]. During EMT, cancer cells acquire a mesenchymal phenotype as they adjust their junctions and assume new signaling pathways which help them resist anoikis, migrate and invade. They are capable of developing "lamellipodia/invadopodia" via actin cytoskeleton rearrangement[4]. Early in EMT, transcription factors ZEB, TWIST, and SNAIL/SLUG are involved. SNAIL, not only promotes EMT but also cancer stem cell properties by increasing interleukin-8 (IL-8) production. The PI3K/Akt pathway, is a key regulator of SNAIL by upregulating SNAIL expression and downregulating its` degradation[5].

EMT is triggered by signals from the tumor microenvironment (TME), according to mounting

 DOI: 10.21608/ejh.2023.188661.1846

evidence[5]. CAFs are a common finding in the TME and are thought to be of various origins, the most common of which is through the trans-differentiation of resident fibroblasts in the TME. This trans-differentiation is thought to be triggered by TGF-β upregulation and the acquisition of a highly contractile phenotype (similar to myofibroblasts) concomitant with the expression of alpha-smooth muscle actin (α-SMA)[6]. CAFs have been shown to undergo frequent genetic changes and to respond to extracellular molecules like cytokines and growth factors[7,8].

Cancer cells and CAFs are constantly communicating in a bidirectional and intricate manner. This crosstalk allows cancer cells to recruit and convert fibroblasts into CAFs, thereby promoting cancer cell progression[9-11]. In recent years, several autocrine and paracrine loops influencing CAF and cancer cell secretomes have been described. The majority of emerging trends in CAF biology point to the fact that CAF-secreted factors are valuable druggable targets[11]. CAFs secrete a significant amount of TGF-β which promotes EMT in epithelial cancer cells and maintains a self-sustaining active state of α-SMA production in myofibroblasts[12].

Furthermore, stimulation of the TGF-/HIF-1 alpha pathway, as well as cancer cell-derived extracellular vesicles (EVs) carrying CXCR-4 mRNA, has been shown to stimulate vascular endothelial growth factor (VEGF) secretion in CAFs[13]. In several cancers, EVs containing miR-10b increase TGF-β expression via the phosphoinositide 3-kinase (PI3K)/protein kinase B (AKT)/mammalian target of rapamycin (mTOR) signaling pathway[11]. TGF-β, on the other hand, is thought to be able to induce the intracellular localization of epidermal growth factor receptor (EGFR), which in turn activates the PI3K/Akt signaling pathway[14]. In turn, the PI3K/AKT pathway encourages CAF differentiation in the TME[13,15].

Beyond tumor progression, the continuous communication between CAFs and cancer cells also leads to drug resistance[16]. On the one hand, CAF exosomes or metabolic components like lactate aid in chemoresistance. While, on the other hand, upregulation of the PI3K/AKT pathway in cancer cells improves drug efflux via ATP-binding cassette (ABC) transporters, thereby decreasing chemotherapeutic drug response[17]. Pre-clinical as well as clinical trials, revealed that the antifungal drug itraconazole (ITZ) may overcome the chemoresistance of cancer cells caused by P-glycoprotein[4,5].

ITZ is an antifungal drug with strong lipophilicity and a track record of safety, and that has been repurposed recently for cancer treatment[18,19]. ITZ has a wide-ranging tissue distribution characterized by tissue concentrations many times higher than plasma, a good absorption rate orally, a fairly long elimination half-life - equivalent to about one day, and bio-transformation into a variety of metabolites in humans[20]. ITZ was discovered by the US Food and Drug Administration (FDA) to be an inhibitor of Sonic Hedgehog (SHh) signaling in 2010 and an anti-angiogenic agent in 2007[21,22]. By lowering sterol carrier protein 2 (SCP2) levels, it has been demonstrated that ITZ can prevent cholesterol from being transported from late endosomes and lysosomes to the plasma membrane. This action suppresses oncogenic pathways like PI3K/AKT/mTOR and Yes-associated protein/transcriptional coactivator with PDZ-binding motif (YAP/TAZ) signaling, activates autophagy, and eventually slows down cell proliferation[22–24].

Earlier research led to the conclusion that α-SMA is a promising prognostic marker in SCC because it showed increased expression with tumor grade in both the TME (more specifically, CAFs) and epithelial cells[4]. This was attributed to the interaction between these two cells, with TGF-β suggested as the primary accountable factor. As a result of the paradoxical function that TGF-β signaling pathway plays in both the suppression and advancement of cancer, this molecule has received extensive attention, over the years and still is to date.

Thereafter, the current work aimed to evaluate the immunohistochemical expression of α-SMA and TGF-β in TSCC biopsied tissue specimens with regard to tumor grade and lymph node involvement. Consequently, ITZ was chosen as a repurposed tested drug for the treatment of TSCC cell line. We aimed to evaluate its effect on α-SMA, TGF-β, and SNAIL as well as VEGF expression and on the migration and invasion ability of SCC-25 cell line. To the best of our knowledge very few papers have been published regarding the effect of ITZ on TSCC.

MATERIAL AND METHODS

Immunohistochemical Expression of α-SMA and TGF-β in Different Grades of TSCC and Clinical Evaluation of Lymph Node Involvement

From the archives of the Oral Pathology Department (from 2011–2019), Faculty of Dentistry, Ain-Shams University, and Faculty of Oral and Dental Medicine, Future University in Egypt, twenty-four paraffin blocks from various grades of TSCC were acquired (retrospectively), after receiving informed consent from the patients, the surgeon while acquiring the biopsy. The mean age of the twenty four patients included was (±) 49 years, with 15 (62.5%) male patients and nine (37.5%) female patients. Two oral pathologists independently evaluated the cases histo-pathologically using H&E-stained sections per Broader's classification. Eight (33.3%) of the cases were found to be well differentiated (WD-TSCC), nine (37.5%) to be moderately differentiated (MD-TSCC), and seven (29.5%) to be poorly differentiated (TSCC) (PD-TSCC). None of the WD-TSCC (0%) and 1(11.1%) of the MD-TSCC and 4 (57.1%) of the PD-TSCC exhibited sentinel lymph node involvement as reported by the surgeons. Immunohistochemical expression of the chosen markers was assessed and associated with clinical lymph node involvement.

The immunohistochemical procedures employing monoclonal antibodies against α-SMA and TGF-β in this study were carried out in Oral Biology Department Lab, Faculty of Dentistry, Ain Shams University. Four micrometer-thick portions of paraffin blocks were cut, mounted, and placed on positively charged glass slides. Sections were deparaffinized with xylene and then rehydrated in graded alcohol. The sections were microwaved in citrate buffer before staining procedures. For immunostaining, a generic kit (Lab Vision) was used. Immunostaining was carried out utilizing the biotin-streptavidin system and the peroxidase-anti-peroxidase approach. 3% hydrogen peroxide was given to the mounted tissue sections to suppress endogenous peroxidase activity. After being primary antibody immunolabeled (Lab Vision), the mounted tissue sections underwent overnight treatment at room temperature. Sections were cleaned with phosphate buffer saline (PBS) and then dried. The sections were first cleaned with PBS before being stained with diaminobenzidine chromogen and the counterstain, which was then dried in graded alcohol. Later, xylene was used to clean the sections before mounting. Using image analysis software, photomicrographs taken with a digital camera (C5060, Olympus) fixed through a C-mount to a light microscope (BX60, Olympus) at a magnification of X40 which used to quantify the area fraction of immunohistochemical expression of α-SMA and TGF-β (Image J, 1.41a, NIH).

Docking (Molecular Modeling)

At the CADD Lab of Pharmaceutical Chemistry Department, Faculty of Pharmacy, Future University in Egypt, conformational models were generated automatically using Discovery Studio (DS) version 4.0 software. The 3D structure of ITZ was built and simulated by applying CHARMM force field and Merch molecular force field (MMFF94) as partial charges. For the in silico investigation of ITZ impact in inhibiting both proteins as anticancer drugs, PI3 Kinase gamma, and AKT proteins were chosen. They were retrieved from the protein data bank with the following codes: (3MJW and 3MVH) from the Research Collaboratory for Structural Bioinformatics (RCSB)[2526].

Both proteins were cleaned, the side chains and missing hydrogens were added, and energy minimization in accordance with the DS methodology was used. Following that, a C-Docker-CHARMM-based approach was used. The protein binding pocket was initially docked with the complexed ligand. The constructed ITZ was then docked to produce 10 binding modes, from which the best binding was chosen based on the lowest amount of (C-Docker interaction energy) attained.

Cell Culture

The procedures and tests involving the cell cultures were performed at VACSERA®, Cairo, Egypt.

WI-38 and SCC-25 Cultures

The human male TSCC (SCC-25) cell line and the human lung fibroblast cell line (WI-38) were grown separately in 75ml flasks of Dulbecco's modified Eagle's medium (DMEM) with 10% fetal bovine serum (FBS), 10 g/ml insulin, and 1% penicillin/streptomycin. Flasks were incubated at 37°C and 5% CO2 in a humid environment.

ITZ (Sporanox®) IC50 Determination on Both Cell Lines

The medicine Sporanox (JANSSEN-CILAG) was bought at a nearby pharmacy. ITZ dosage per capsule is 100 mg. In 96-well plates, each cell line was grown independently for 24 hours at a density of 1.2-1.8 x 104 cells/well in 100 l complete media (n=6). The medication was then diluted in 100 l of 0.1% DMSO/PBS and serially diluted to different concentrations (100, 25, 6.25, 1.56, and 0.39 M) before being put into the cell wells in a total volume of 200 l. Blank DMSO solutions were injected into control wells. After 48 and 72 hours, the vitality of the cells was evaluated.

The old media was removed after the incubation period, and cells were then washed in PBS. Each well then received a fresh 100 µl of medium (phenol red and serum-free), followed by 10 µl of MTT reagent. At 37°C and 5% CO2, the plates were incubated for two hours. Following the removal of all media, 100 µl of the solubilization solution (the solution used to dissolve the formazan crystals) was added. Each plate's spectrophotometric absorbance was evaluated at 570 nm in a plate reader (ROBONIK P2000).

Co-culture

In two 75 ml flasks, the WI-38 and SCC-25 cell lines were co-cultured for nine days in the same complete media. Flasks were incubated at 37°C and 5% CO2 in a humid environment. ITZ was introduced to one of the flasks on day eight of co-culturing at a concentration of 10 mol for the remainder of the co-culture period (last 48 hours). After nine days of cell culture, the media from the co-culture with and without treatment was removed, and SCC-25 was independently cultured in groups I and II, respectively as shown (Table 1).

Table 1: Experimental design and grouping

Group I	SCC-25 cultured in medium obtained from co-cultured SCC-25 with WI-38 for 9 days without treatment.
Group II	SCC-25 cultured in medium obtained from co-cultured SCC-25 with WI-38 for 9 days with 48 hrs of ITZ treatment.

Molecular Testing for Groups I and II (RT-PCR for α-SMA, TGF-β, VEGF, and SNAIL)

Using a Qiagen RNeasy extraction kit (#74004), RNA was isolated. 1x106 SCC-25 cells from groups I and II of the manufacturer's protocol were disrupted and homogenized in buffer RLT. On a Rotor-gene Q cycler system, extracted RNA was reverse-transcribed and amplified using the BIORAD iScript one-step RT-PCR kit with SYBR green

(#345-0412). (Qiagen). Housekeeping genes such as beta-actin and GAPDH were employed as primers, and each group's levels of -SMA, TGF-, SNAIL, and VEGF were also measured (Table 2).

Table 2: The primers sequences used

Gene	Forward	Reverse
GAPDH	5′- GAAGGTGAAGGTCGGAGT -3′	5′- CATGGGTGGAATCATATTGGAA -3′
B-actin	5'- TCGCCATTATCCCCAGCAAGAAG -3'	5'- TGGTGTCGGGATCCACCTCAATGA -3'
α-SMA	5′- GCATCCACGAAACCACCTA -3′	5’- CACGAGTAACAAATCAAAGC -3’
TGF-β	5'- GTCCCCTTGCCTGGAAAGATAC -3'	5'- GGTCTGTGATTACAAACCCCTTCTG -3'
SNAIL	5'- GCTGCAGGACTCTAATCCAGAGTT -3'	5'- GACAGAGTCCCAGATGAGCATTG -3'
VEGF	5'- AAGCCAGCACATAGGAGAGATGA -3'	5'- TCTTTCTTTGGTCTGCATTCACA -3'

Cell Migration and Invasion Assay

The capacity of SCC-25 cells in Groups I and II to migrate and invade was evaluated. Cells in serum-free media were planted with 2–5 x 104 cell density per well in transwell permeable inserts with 8 m diameter size pores in 96-well plates to test their ability to migrate. The cells were allowed to settle for 10 minutes before a full medium including serum was introduced to the receiver well. In a humid environment, plates were incubated for 24 hours in a humid environment at 37°C and 5% CO2.

Basement membrane extract (BME) (Cultrex, Trevigen) was applied to the transwell insert membranes before cell seeding to assess the cells' propensity for invasion. Briefly, after being prepared following the manufacturer's instructions and filtered through a 0.2-m filter, 50 l of the BME solution was added to the top of each insert's membrane/well of the 96-well plate. Inserts used as controls lacked any coating. Plates were incubated at 37°C and 5% CO2 throughout the night to produce coat gel. Cells were then plated on the permeable coated inserts at a density of 5x104/well in serum-free medium. In the receiver well, 150 l of complete media containing serum were added after the cells had been allowed to settle for 10 minutes. For 24 hours, plates were incubated. Plates were incubated for 24 hrs at 37°c and 5% CO2 in a humidified atmosphere.

After incubation, non-migrated/non-invaded cells were removed from the inside of the inserts by swabbing with clean cotton swabs from the upper side. Each insert/well was then filled with 100 l of crystal violet stain, and the plate was let to stand for 10 minutes to allow the staining of the cells. The additional stain was then removed from the inserts by washing them in water. After letting the inserts dry, they were examined under a light microscope. The number of invading cells was recorded.

Statistical Analysis

Utilizing the statistical program for social sciences, version 20.0, recorded data was examined. The mean and standard deviation were used to express quantitative data (SD). Frequency and percentage were used to express qualitative data. When comparing more than two means, one-way analysis of variance (ANOVA) was employed. Least Significant Difference (LSD), a post-hoc test, was employed for several comparisons between various variables. When contrasting between s, the independent-samples t-test of significance was employed. With a 5% acceptable margin of error and a 95% confidence interval. *P-values* 0.05 and 0.001 were regarded as significant and very significant, respectively.

RESULTS

Immunohistochemical and Clinical Results

Figures (1-6) displayed the location of the expression of α-SMA and TGF-β in the immunohistochemically stained sections, whereas (Figures 7, Table 3) displayed the mean area fractions. ANOVA showed that there was a significant difference between the mean area fractions of α-SMA and TGF-β expressions. In contrast, the expression of α-SMA was considerably higher in the PD-SCC and the difference in its expression between the WD-SCC and MD-SCC was not statistically significant, according to post hoc data.

Microscopic evaluation demonstrated that WD-TSCC specimens showed immunopositivity in the stromal cells and immunonegativity in neoplastic epithelial cell nests for both α-SMA and TGF-β. MD-TSCC specimens showed nuclear, cytoplasmic and membranous immunopositivity in the neoplastic epithelial cell nests with TGF-β, whereas alot of the neoplastic epithelial cells were immunonegative with α-SMA and spindle cells in close proximity to the neoplastic epithelial nests were immunopositive. PD-TSCC specimens exhibited cytoplasmic, membranous as well as nuclear immunopositivity in the majority of neoplastic epithelial cells with TGF-β, while neoplastic epithelial cells nuclei were mostly immunonegative with α-SMA (Figures 1-6).

(Table 4) displays the lymph node involvement in the various instances considered in this investigation. Between the various SCC grades, there was a statistically significant variation in the proportion of instances involving lymph nodes. The comparison between the mean area fraction of immunohistochemical expression of α-SMA and TGF-β in cases with lymph node involvement and cases without lymph node involvement revealed statistically significant differences.

Molecular Docking Results

Docking study was started first by configuring

the binding mode of the bioactive conformer of the co-crystallized ligand with PI3 Kinase gamma; (benzofuranone) and that of AKT; (N-{[(3S)-3-amino-1-(5-ethyl-7H-pyrrolo[2,3-d]pyrimidin-4-yl)pyrrolidin-3-yl] methyl}-2,4-difluoro enzamide) which were exempted after applying C-Docker protocol in Discovery studio 4.0 software program. The bioactive conformer of the benzofuranone displayed Pi-bond interaction via its aromatic rings with Asp 788 and also showed hydrogen bond formation between hydroxyl group of benzofuranone and Glu 856 as shown in (Figure 7). The -(C-Docker interaction energy) obtained for benzofuranone complexed with PI3 Kinase was -39.123 Kcal/mol.

On the other hand, when ITZ was docked with PI3 Kinase, it showed better -(C-Docker interaction energy)= -65.657 Kcal/mol with enhanced binding mode than the co-crystallized complex. ITZ showed Pi-bond interactions between its aromatic ring and Asp788 and between its triazole ring and Glu 856, while its other aromatic ring and carbonyl group showed extra Pi-bond and hydrogen bond respectively with Arg 277 as shown in (Figure 8).

Meanwhile, the bioactive conformer pyrrole-benzamide derivative displayed binding with AKT protein in the form of a hydrogen bond between fluorine atom and His 194, a Pi-bond between aromatic ring and Glu 191, and three hydrogen bonds between; other fluorine atoms and Lys 179, carbonyl of amide group and Lys 179, nitrogen of pyrrole ring and Lys 277 as shown in (Figure 9). The (C-Docker interaction energy) of pyrrole-benzamide derivative was -43.683 Kcal/mol. ITZ displayed comparable binding when docked with AKT; where triazolone ring formed hydrophobic binding with His 194 and non-covalent binding with Cys 310 as shown in (Figure 10). Also, aromatic ring formed another hydrophobic binding with Phe 438. The -(C-Docker interaction energy) of ITZ docked with AKT was -58.02 Kcal/mol.

RT-PCR α-SMA, TGF-β, SNAIL and VEGF Gene Expression, Migration and Invasion Assay Results

Using student t-test, group I showed significantly higher expression ($p<0.05$) of all studied genes (α-SMA, TGF-β, SNAIL and VEGF) as well as higher invading and migrating ability of the TSCC cells than for group II as shown in (Table 5).

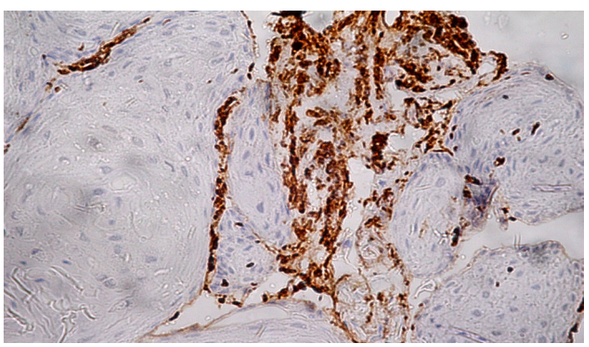

Fig. 1: A photomicrograph of a WD-TSCC specimen showing immunopositivity in the stromal cells (yellow arrow) and immunonegativity in neoplastic epithelial cell nests (red arrow) (TGF-β, original magnification x40).

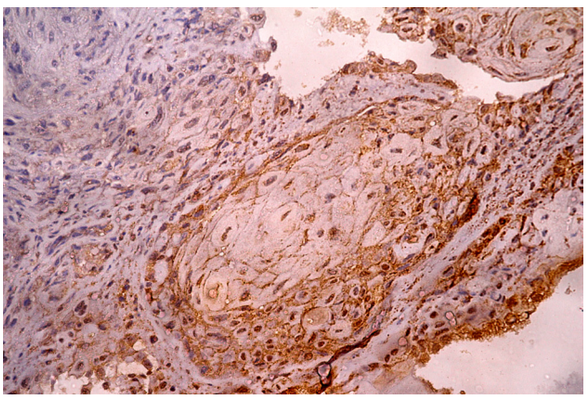

Fig. 2: A photomicrograph of MD-TSCC showing cytoplasmic and membranous immunopositivity in the neoplastic epithelial cell nests (yellow arrow). Most of the nuclei in the neoplastic epithelial cell nests exhibited immunopositivity. Note: the immunopositivity appeared to be relatively more intense in the peripheral cells of the cell nests than in the inner neoplastic epithelial cells (TGF-β, original magnification x40).

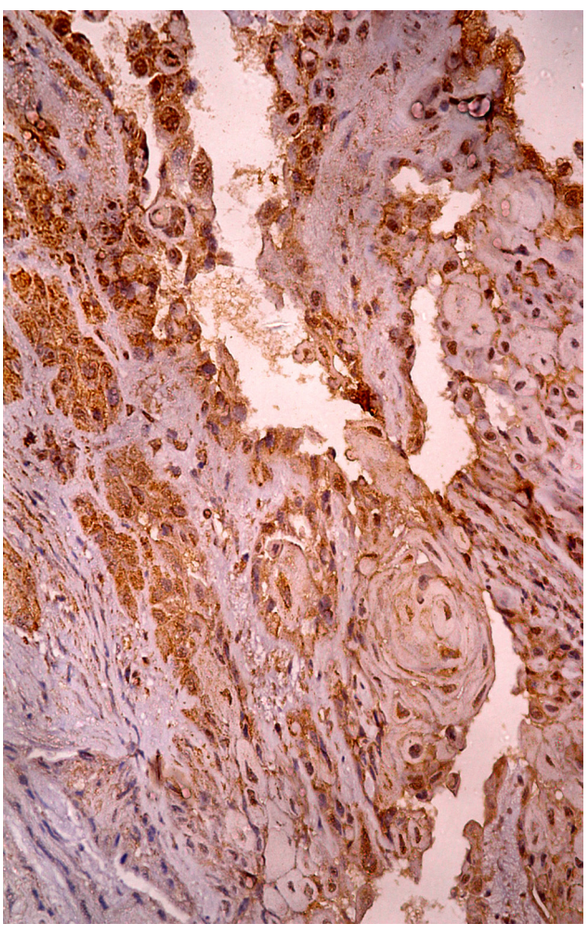

Fig. 3: A photomicrograph of a PD-SCC specimen showing cytoplasmic, membranous as well as nuclear immunopositivity in the majority of neoplastic epithelial cells (red arrow). Some spindle stromal cells exhibiting immunopositivity (yellow arrow) were also noted (TGF-β, original magnification x40).

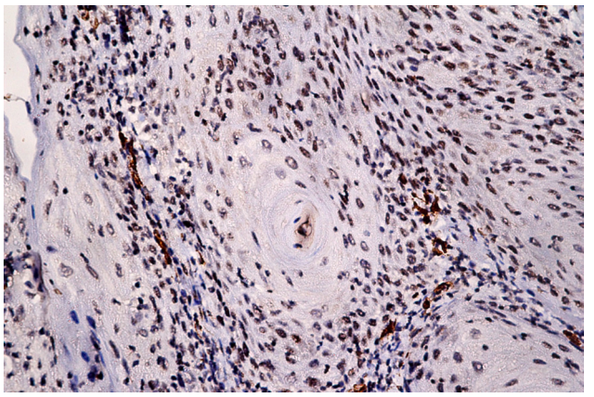

Fig. 4: A photomicrograph of a WD-TSCC specimen showing immunopositivity in some of the stromal cells (yellow arrow) near immunonegative neoplastic epithelial cell nests (red arrow) (α-SMA, original magnification x40).

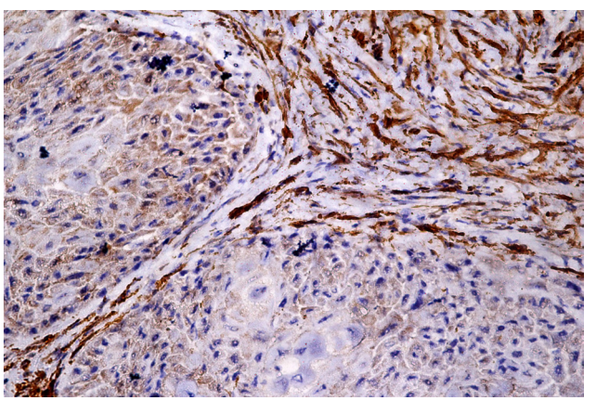

Fig. 5: A photomicrograph of an MD-TSCC specimen showing cytoplasmic and membranous immunopositivity in some of the neoplastic epithelial cell nests (yellow arrow) while alot of the neoplastic epithelial cells were immunonegative (red arrow). Note: immunopositive spindle cells in close proximity to the neoplastic epithelial nests (black arrow) (α-SMA, original magnification x40).

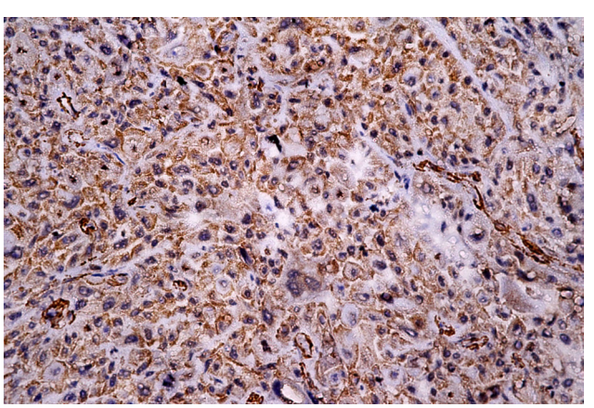

Fig. 6: A photomicrograph of a PD-SCC specimen showing cytoplasmic and membranous immunopositivity in the majority of neoplastic epithelial cells (yellow arrow). Neoplastic epithelial cells nuclei were mostly immunonegative (red arrow) (α-SMA, original magnification x40).

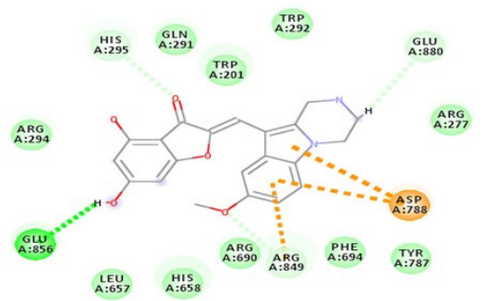

Fig. 7: 2D-interaction binding mode between benzofuranone and PI3 Kinase. Orange dotted lines reflect Pi-bonding while green dotted lines reflect hydrogen bonds.

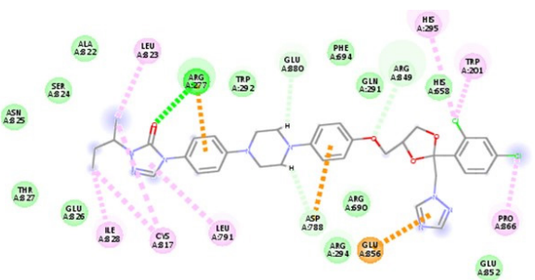

Fig. 8: 2D-interaction binding mode between ITZ and PI3 Kinase. Orange dotted lines reflect Pi-bonding while green dotted lines reflect hydrogen bonds.

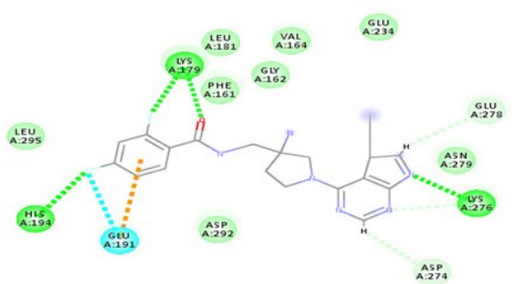

Fig. 9: 2D-interaction binding mode between Pyrrolo-benzamide derivative and AKT. Orange dotted lines reflect Pi-bonding while green dotted lines reflect hydrogen bonds. Cyan dotted lines are the formation of water.

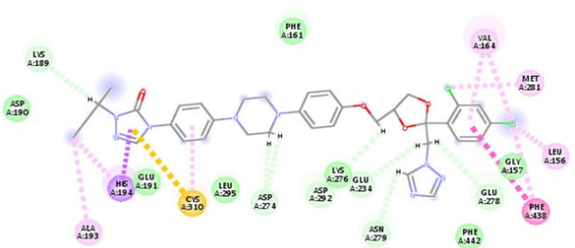

Fig. 10: 2D-interaction binding mode between ITZ and AKT. Dark purple dotted lines reflect hydrophobic interactions. Yellow dotted lines reflect non-covalent bonding while light purple dotted lines reflect electrostatic interactions.

Table 3: ANOVA and Post Hoc for comparison between mean area fraction ±SD of immunohistochemical expression of α-SMA and TGF-β and clinical lymph node involvement in different grades of TSCC

Markers	WD-SCC	MD-SCC	PD-SCC	ANOVA *p-value*
α-SMA	13.69±2.13	20.00±4.36	43.54±11.43#‡	<0.001**
TGF-β	25.42±2.45	35.31±1.70#	39.49±3.49#‡	<0.001**
No lymph node involvement	8 (100%)	8 (88.9%)	3 (42.9%)	0.016*
Lymph node involvement	0 (0%)	1 (11.1%)	4 (57.1%)	

Post Hoc: # significant difference with WD-SCC; ‡ significant difference with MD-SCC *p-value*>0.05 NS; **p-value* <0.05 S; ***p-value* <0.001 HS

Table 4: Post Hoc comparison between mean area fraction ±SD of immunohistochemical expression of α-SMA and TGF-β in cases with and without clinical lymph node involvement in different grades of TSCC

Markers	Lymph node involvement		t-test
	Involved	Not involved	*p-value*
α-SMA	36.84±11.20	21.58±13.33	0.019*
TGF-β	37.75±2.72	32.05±6.59	0.029*

Table 5: Independent sample t-test for comparison of mean fold changes ±SD of genes expression as well as invasion and migration ability between group I and group II

	Group I	Group II	*p-value*
α-SMA	0.79±0.09	0.47±0.08	0.010*
TGF-β	12.08±4.26	1.08±0.17	0.011*
SNAIL	1.78±0.19	0.40±0.07	<0.001**
VEGF	2.01±0.34	0.58±0.15	0.003*
Invasion	31.77±0.57	13.03±0.50	0.0001**
Migration	19.77±0.31	6.17±0.31	0.0001**

**p-value* <0.05 S; ***p-value* <0.001 HS

Discussion

TSCC is increasing in incidence and is associated with aggressive clinical behavior and poor prognosis. Several studies have been conducted to determine whether the CAFs secretome could be used to predict a cancer patient's prognosis and responsiveness to therapy.

According to research, CAFs can release TGF-β, both in *vitro* and in *vivo*, the paracrine TGF-β signaling pathway promote cancer migration and invasion[11]. In our study, immunohistochemical analysis revealed that the expression of α-SMA and TGF-β in WD-TSCC specimens was in the TME rather than in the tumor cells and that they were expressed in the stroma in close proximity to the invasive epithelial cells. Conversely, in PD-TSCC the expression of these markers was upregulated in the tumor cells themselves, with concurrent increased cases with LN involvement. This may be attributed to the fact that overexpression of α-SMA is thought to be necessary for EMT in SCC. In the work done by Kenta Haga, *et al*, 2021[27], they reported that TGF-β positive fibroblasts were found in the stroma of TSCC and were distributed similarly to α-SMA -positive CAFs. Additionally, they demonstrated that α-SMA and TGF-β might be used as possible indicators of CAFs in the TME, our study's findings further support these conclusions.

Finding a “cure” for cancer is the ultimate aim of all cancer research. Hence, moving forward from the above-mentioned deductions and the conclusions of our previous work[4], ITZ was chosen to study its effect as a potential therapeutic agent for TSCC. It has favorable pharmacokinetics, is affordable, already on the market, approved and clinically tried for other ailments[18,22,28]. Re-purposing ITZ for cancer treatment has been studied and has given promising results[18,21]. In our study, molecular docking was performed, and it was found that ITZ was able to interact strongly with PI3/AKT proteins in addition to its previously reported effect on the SHh signaling pathway. It is suggested that ITZ has a remarkable inhibitory activity for both PI3 kinase and AKT proteins compared to other complex ligand inhibitors, which ensures the anticancer activity of ITZ. PI3/AKT signaling has been linked to both α-SMA and TGF-β expressions and CAFs differentiation and is a key player in, chemotherapeutic resistance, EMT activation and tumor cell migration[5,22,29–32].

ITZ is not only well tolerated with fewer side effects than cytotoxic drugs, but it is also very promising to be used as an adjuvant to other chemotherapeutic agents[19,22], as it is expected to reduce cancer cell resistance to therapy and potentiate the therapeutic effect of the drug used with it, via its inhibition of the PI3/AKT signaling pathway and down-regulation of drug efflux by ABC transporters[17].

To evaluate its effect in *vitro* ITZ was applied to TSCC cell line that has been cultured in a medium presumably rich in factors secreted by CAFs -refer to our previous work[4]

as most emerging trends in CAF biology draw attention to CAF-secreted factors as druggable targets[11]. In the current work, TSCC cells cultured in a medium rich with CAF-secreted factors were evaluated and compared to the TSCC cells that were cultured with added ITZ treatment.

The ITZ-treated group exhibited lower expression of α-SMA, TGF-β, and SNAIL, which are all markers of EMT, compared to the non-treated group. This result may be attributed to the abrogation of the AKT signaling pathway by ITZ. In cancer, over-activation of AKT phosphorylates GSK-3beta inducing its proteolytic removal. This increases the stability of SNAIL, the negative transcription factor, consequently decreasing the transcription of the transmembrane protein E-cadherin with upregulation of TGF-β and subsequent α-SMA expression. These changes collectively permitting cancer cell detachment, EMT and metastases[30]. Moreover, as discussed earlier, ITZ has been proven to inhibit myofibroblastic differentiation and α-SMA expression[28]. In addition, the down regulation of the genes mentioned above, may be brought about via IITZ-induced delayed trafficking of cholesterol from lysosomes and endosomes to the plasma membrane, resulting in subsequent suppression of AKT-MTOR signaling[33]. The invasion and migration assay results in this study further elaborated the global effect of ITZ on the cultured TSCC cells beyond individual gene expressions, where the ITZ-treated group significantly exhibited fewer invading and migrating cells.

In this study, the expression of VEGF was also assessed because the VEGF family has a role in lymphatic metastasis. It was discovered that the ITZ-treated group had considerably lower VEGF expression than the control group. This is in line with the findings of Nacev *et al*. (2011) who noted that ITZ's capacity to reduce angiogenesis seems to be related to both its antifungal properties and the suppression of the Hedgehog (Hh) pathway, which results in decreased endothelial cell proliferation. ITZ reduces endothelial cell proliferation by preventing VEGF from binding to the VEGF receptor 2. This lowers VEGF signaling. ITZ can also prevent the creation of tubes, chemotaxis, and cell migration, all of which are necessary for neovascularization and angiogenesis[34].

From the results of this study, it was concluded that ITZ can reduce the expression of α-SMA, TGF-β, SNAIL and VEGF in TSCC and to down-regulate its invasion and migration ability in *vitro*. So, it was recommended that ITZ is a promising chemotherapeutic agent that requires additional researching before being applied in *vivo*. Further studies are required to test its full range of applications in cancer research.

CONFLICT OF INTERESTS

There are no conflicts of interest.

REFERENCES

1. Dayan D, Salo T, Salo S, Nyberg P, Nurmenniemi S, Costea DE, *et al*.: Molecular crosstalk between cancer cells and tumor microenvironment components suggests potential targets for new therapeutic approaches in mobile tongue cancer. Cancer Med. (2012) 1(2):128–40. doi: 10.1002/cam4.24
2. Voss JO, Freund L, Neumann F, Mrosk F, Rubarth K, Kreutzer K, *et al*.: Prognostic value of lymph node involvement in oral squamous cell carcinoma. Clin Oral Investig. (2022) 26(11): 6711–6720 doi: 10.1007/s00784-022-04630-7
3. El-Kammar H, Ghazy SE: Synergistic effect of combined treatment with extra virgin olive oil and doxorubicin on squamous cell carcinoma cell line. Egypt Dent J. (2018) 64:3407–16. doi 10.21608/EDJ.2018.79058
4. El-Kammar H, Afifi NS and AbdulKhalik D: Role of alpha smooth muscle actin in oral squamous cell carcinoma progression. Egypt Dent J. (2019) 65:2387–96. doi: 10.21608/EDJ.2019.72277
5. Li H, Zhang J, Chen S-W, Liu L, Li L, Gao F, *et al*.: Cancer-associated fibroblasts provide a suitable microenvironment for tumor development and progression in oral tongue squamous cancer. J Transl Med. (2015) 13(1):1–10. . doi: 10.1186/s12967-015-0551-8
6. Bellomo C, Caja L and Moustakas A. Transforming growth factor β as regulator of cancer stemness and metastasis. Br J Cancer. (2016) 115(7):761–9. doi: 10.1038/bjc.2016.255
7. Lee YT, Tan YJ, Falasca M and Oon CE: Cancer-associated fibroblasts: epigenetic regulation and therapeutic intervention in breast cancer. Cancers (Basel). (2020) 12(10):2949. doi: 10.3390/cancers12102949
8. Mishra R, Haldar S, Suchanti S and Bhowmick NA: Epigenetic changes in fibroblasts drive cancer metabolism and differentiation. Endocr Relat Cancer. (2019) 26(12):R673–88. doi: 10.1530/ERC-19-0347
9. He C, Wang L, Li L and Zhu G: Extracellular vesicle-orchestrated crosstalk between cancer-associated fibroblasts and tumors. Transl Oncol. (2021) 14(12):101231. DOI: 10.1016/j.tranon.2021.101231
10. Muchlińska A, Nagel A, Popęda M, Szade J, Niemira M, Zieliński J, *et al*.: Alpha-smooth muscle actin-positive cancer-associated fibroblasts secreting osteopontin promote growth of luminal breast cancer. Cell Mol Biol Lett. (2022) 27(1):1–14. DOI: 10.1186/s11658-022-00351-7
11. Linares J, Marín-Jiménez JA, Badia-Ramentol J and Calon A: Determinants and functions of CAFs secretome during cancer progression and therapy. Front Cell Dev Biol. (2021) 8:621070. DOI: 10.3389/fcell.2020.621070

12. Yu Y, Xiao CH, Tan L, Wang QS, Li XQ and Feng Y: Cancer-associated fibroblasts induce epithelial–mesenchymal transition of breast cancer cells through paracrine TGF-β signalling. Br J Cancer. (2014) 110(3):724–32. DOI: 10.1038/bjc.2013.768

13. Kim I, Choi S, Yoo S, Lee M and Kim I: Cancer-associated fibroblasts in the hypoxic tumor microenvironment. Cancers (Basel). (2022) 14(14):3321. DOI: 10.3390/cancers14143321

14. Xu W, Yang Z and Lu N: A new role for the PI3K/Akt signaling pathway in the epithelial-mesenchymal transition. Cell Adh Migr. (2015) 9(4):317–24. doi: 10.1080/19336918.2015.1016686

15. Wu F, Yang J, Liu J, Wang Y, Mu J, Zeng Q, *et al*.: Signaling pathways in cancer-associated fibroblasts and targeted therapy for cancer. Signal Transduct Target Ther. (2021) 6(1):218. DOI: 10.1038/s41392-021-00641-0

16. Ramos A, Sadeghi S and Tabatabaeian H: Battling chemoresistance in cancer: root causes and strategies to uproot them. Int J Mol Sci. (2021) 22(17):9451. doi: 10.3390/ijms22179451

17. Liu R, Chen Y, Liu G, Li C, Song Y, Cao Z, *et al*.: PI3K/AKT pathway as a key link modulates the multidrug resistance of cancers. Cell Death Dis. (2020) 11(9):1–12. DOI:10.1038/s41419-020-02998-6

18. Pounds R, Leonard S, Dawson C and Kehoe S: Repurposing itraconazole for the treatment of cancer. Oncol Lett. (2017) 14(3):2587–97. doi: 10.3892/ol.2017.6569

19. Deng H, Huang L, Liao Z, Liu M, Li Q and Xu R: Itraconazole inhibits the Hedgehog signaling pathway thereby inducing autophagy-mediated apoptosis of colon cancer cells. Cell Death Dis. (2020) 11(7):1–15. doi: 10.1038/s41419-020-02742-0

20. Mahajan H, Jain GK, Dhoot D, Deshmukh GA and Barkate HV: Serum and sebum pharmacokinetics evaluation of a novel formulation of itraconazole in healthy volunteers. Indian J Drugs Dermatology. (2022) 8(1):7. DOI: 10.4103/ijdd.ijdd_23_21

21. Tsubamoto H, Ueda T, Inoue K, Sakata K, Shibahara H and Sonoda T: Repurposing itraconazole as an anticancer agent. Oncol Lett. (2017) 14(2):1240–6. DOI: 10.3892/ol.2017.6325

22. Tsubamoto H, Inoue K, Sakata K, Ueda T, Takeyama R, Shibahara H, *et al*.: Itraconazole inhibits AKT/mTOR signaling and proliferation in endometrial cancer cells. Anticancer Res. (2017) 37(2):515–9. doi: 10.21873/anticanres.11343.

23. Isono R, Tsubamoto H, Ueda T, Takimoto Y, Inoue K, Sakata K, *et al*.: Itraconazole inhibits intracellular cholesterol trafficking and decreases phosphatidylserine level in cervical cancer cells. Anticancer Res. (2021) 41(11):5477–80. doi: 10.21873/anticanres.15360

24. Vona R, Iessi E and Matarrese P: Role of cholesterol and lipid rafts in cancer signaling: a promising therapeutic opportunity? Front Cell Dev Biol. (2021) 9:622908. doi.org/10.3389/fcell.2021.622908

25. Freeman-Cook KD, Autry C, Borzillo G, Gordon D, Barbacci-Tobin E, Bernardo V, *et al*.: Design of selective, ATP-competitive inhibitors of Akt. J Med Chem. (2010) 53(12):4615–22. doi: 10.1021/jm1003842

26. Zhang N, Ayral-Kaloustian S, Anderson JT, Nguyen T, Das S, Venkatesan AM, *et al*.: 5-Ureidobenzofuranone indoles as potent and efficacious inhibitors of PI3 kinase-α and mTOR for the treatment of breast cancer. Bioorg Med Chem Lett. (2010) 20(12):3526–9. doi: 10.1016/j.bmcl.2010.04.139

27. Haga K, Yamazaki M, Maruyama S, Kawaharada M, Suzuki A, Hoshikawa E, *et al*.: Crosstalk between oral squamous cell carcinoma cells and cancer-associated fibroblasts via the TGF-β/SOX9 axis in cancer progression. Transl Oncol. (2021) 14(12):101236. doi: 10.1016/j.tranon.2021.101236.

28. Kim JS, Cho KS, Park SH, Lee SH, Lee JH, Jeong KH, *et al*.: Itraconazole attenuates peritoneal fibrosis through its effect on the sonic hedgehog signaling pathway in Mice. Am J Nephrol. (2018) 48(6):456–64. doi: 10.1159/000493550

29. Takahashi H, Rokudai S, Kawabata-Iwakawa R, Sakakura K, Oyama T, Nishiyama M, *et al*.: AKT3 is a novel regulator of cancer-associated fibroblasts in head and neck squamous cell carcinoma. Cancers (Basel). (2021) 13(6):1233. doi: 10.1159/000493550.

30. Qiao M, Sheng S and Pardee AB: Metastasis and AKT activation. Cell cycle. (2008) 7(19):2991–6. doi: 10.4161/cc.7.19.6784.

31. Bollong MJ, Yang B, Vergani N, Beyer BA, Chin EN, Zambaldo C, *et al*.: Small molecule-mediated inhibition of myofibroblast transdifferentiation for the treatment of fibrosis. Proc Natl Acad Sci. (2017) 114(18):4679–84. doi.org/10.1073/pnas.1702750114

32. Porta C, Paglino C and Mosca A: Targeting PI3K/Akt/mTOR signaling in cancer. Front Oncol. (2014) 4:64. doi: 10.3389/fonc.2014.00064

33. Liu R, Li J, Zhang T, Zou L, Chen Y, Wang K, *et al*.: Itraconazole suppresses the growth of glioblastoma through induction of autophagy: involvement of abnormal cholesterol trafficking. Autophagy. (2014) 10(7):1241–55. doi: 10.4161/auto.28912

34. Nacev BA, Grassi P, Dell A, Haslam SM and Liu JO: The antifungal drug itraconazole inhibits vascular endothelial growth factor receptor 2 (VEGFR2) glycosylation, trafficking, and signaling in endothelial cells. J Biol Chem. (2011) 286(51):44045–56. doi: 10.1074/jbc.M111.278754.

الملخص العربى

الايتراكونازول: علاج كيميائي واعد معاد التوظيف لسرطان اللسان

هالة الكمار[١]، محمد عمار[٢]، ايتن فوزي[٣]، دينا عبد الخالق[٤]، نيرمين عفيفي[٤]

[١]قسم باثولوجيا الفم، كلية طب الفم والاسنان، جامعة المستقبل بمصر

[٢]قسم المواد الحيوية، كلية طب الفم والاسنان، جامعة المستقبل بمصر

[٣]قسم الكيمياء الصيدلانية، كلية الصيدلة، جامعة المستقبل بمصر

[٤]قسم بيولوجيا الفم، كلية طب الاسنان، جامعة عين شمس

الخلفية: ان البحث عن علاجات كيميائية مبتكرة ضد السرطان يعد أمرًا مرغوبًا فيه ، ولكنه ليس مثاليًا من حيث التكلفة والوقت. وبالتالي فإن إعادة توظيف الأدوية الحالية لعلاج السرطان أصبح أكثر جاذبية. إيتراكونازول (ITZ) هو دواء مضاد للفطريات تم إعادة توظيفه كعامل مضاد للسرطان للعديد من أنواع السرطان. هناك حديث متبادل ثنائي الاتجاه ومعقد مستمر بين الخلايا السرطانية والخلايا الليفية المرتبطة بالسرطان (CAFs). معظم الاتجاهات الناشئة في بيولوجيا CAFتلفت الانتباه إلى العوامل التي تفرزها CAF كمستهدفات للعلاج الدوائي. تم ربط إشارات المسار PI٣ / AKT بظهور كل من α-SMA و TGF-وتمايز CAFs وهي لاعب رئيسي في مقاومة العلاج الكيميائي.

الأهداف من الدراسة: كان الهدف من هذه الدراسة هو ربط التعبير الكيميائي الهيستولوجي المناعي لـ α-SMA كعلامة لـ CAF و TGF-كعلامة للغزو مع درجة الورم وامتداده للعقد الليمفاوية في عينات سرطان الخلايا الحرشفية اللسان (TSCC) وتقييم تأثير ITZ على الغزو والورم الخبيث لخط خلية TSCC.

المواد والطرق: تم تقييم التعبير الكيميائي المناعي لـ α-SMA و TGF-في أربعة وعشرين عينة من درجات مختلفة من TSCC والامتداد للعقد الليمفاوية بأثر رجعي. و تم إجراء الالتحام الجزيئي لـ ITZ مع PI٣ / AKT وتم تقييم تأثيره على خط خلية SCC-٢٥ المزروع في الوسط الذي تم الحصول عليه من الزراعة المشتركة لـ WI-٣٨ (الخلايا الليفية الطبيعية) وخطوط الخلايا SCC-٢٥. وتم تقييم التعبير عن جينات α-SMA و β-TGF و SNAIL و VEGF بالإضافة إلى القدرة على الغزو والهجرة.

النتائج: كان التعبير الهيستوكيميائي المناعي لـ α-SMA و TGF-أعلى بشكل ملحوظ في الحالات التي تظهر تورط العقد الليمفاوية. أظهرت المجموعة المعالجة بـ ITZ قدرة أقل على الهجرة والغزو بالإضافة إلى تعبيرات اقل من α-SMA و β-TGF و SNAIL و VEGF مقارنة بالمجموعة الغير معالجة.

الاستنتاج: الايتراكونازول له القدرة على تثبيط غزو و هجرة خط خلايا سرطان الخلايا الحرشفية للسان.